

UNSTEADY GROUND EFFECTS ON THE AERODYNAMIC COEFFICIENTS OF THICK AIRFOILS

A. O. Nuhait* and M.F. Zedan

*Mechanical Engineering Department
King Saud University
Riyadh, Saudi Arabia*

الخلاصة :

تمّ تعديل أنموذج عددي مبني على طريقة الصور المعكوسة أستنبط سابقا لحساب السريان غير المستقر حول الألواح المحدبة التي تطير بالقرب من الأرض وذلك لكي يمكن تطبيقه على مقاطع الأجنحة السميكة . يشتمل هذا التعديل على تمثيل المقطع وصورته برقائق سطحية ذات دوامية متغيرة خطياً . ولتحقيق « شرط كوتا » تتوالد الدوامات من مؤخرة المقطع مكونة مخرا ينمو مع الوقت .

واستخدم الأنموذج المعدل لدراسة تأثير نسبة السماكة وشكل المقطع وكذلك موقع أقصى السماكة على التغيرات في المعاملات الايروديناميكية وذلك عندما يقترب المقطع من الأرض بالمقارنة بقيمها بعيدا عن الأرض . أظهرت النتائج أن تأثير السماكة على التغيرات في المعاملات الأيروديناميكية يكون صغيرا عندما تكون مقدمة المقطع أقرب إلى الأرض من مؤخرته وتعارض هذه النتيجة مع النتائج المستنبطة باستخدام طريقة التأثير الأرضي المستقر التي تظهر تأثيرات عالية لسماكة المقطع ، أما عندما تكون مقدمة المقطع أبعد عن الأرض من مؤخرته فقد أظهرت النتائج الحالية أن التغيرات في المعاملات تقل بالقرب من الأرض كلما زادت نسبة السماكة وهذا يتفق مع نتائج طريقة السريان المستقر . يمكن عزو النتيجة المشار إليها الى تأثير التفريغ (الشفط) على السطح الأسفل للمقطع الناتج عن « تأثير فينشوري » عندما يكون المقطع قريبا جداً من الأرض ويتفق هذا التفسير مع نتائج حسابات توزيع الضغط على المقطع .

*Address for correspondence:

Chairman, Mechanical Engineering Department
College of Engineering
King Saud University
P.O. Box 800, Riyadh 11421, Saudi Arabia

ABSTRACT

A model based on the image technique developed previously to compute the unsteady potential flow around cambered plates moving near the ground was extended to handle airfoils with thickness. The airfoil and its image were represented by panels with linearly varying vorticity. A wake that grew with time was formed as a result of vortex shedding from the trailing edge to satisfy the unsteady Kutta condition. The model was used to study the effects of airfoil thickness ratio, position of maximum thickness and thickness profile shape on the relative deviations in the aerodynamic coefficients (from their values far from ground) as the airfoil approaches the ground. For negative pitch angles, *i.e.* nose below trailing edge, the results indicated that thickness effects on the relative deviations are generally very small. This is in sharp disagreement with the results in steady ground effect, which indicated substantial thickness effects. When the pitch angle is positive, the relative deviations were observed to drop near ground with increasing thickness ratio in agreement with the trends obtained by using the steady approach. This trend was attributed to suction on the lower surface of the airfoil caused by a "Venturi effect" very close to the ground, as demonstrated by computed pressure distributions.

UNSTEADY GROUND EFFECTS ON THE AERODYNAMIC COEFFICIENTS OF THICK AIRFOILS

INTRODUCTION

At the beginning of the twentieth century, it was observed that airplanes take off easily and tend to “float” during landing. This phenomenon has been called ground effect for obvious reasons. Ground effect was found to increase the lift force coefficient above its value far from ground, in general. Such an increase is utilized in designing wingships which “fly” (or “skim”) between 6 and 30 meters above sea [1]. Extensive research, both theoretical and experimental, was conducted in order to understand and predict the ground effect phenomena as reviewed in the next section. Because of the high expense needed in terms of time and resources, systematic and parametric studies are not well suited for experimental work especially when the number of parameters is not small. For such studies, theoretical or computational investigations are much more convenient provided that reliable and proven models exist. Experimental verification of the results of such studies is still needed.

The ground effect problem is a classical example of this. The parameters affecting the change in aerodynamic coefficients at various levels as the ground is approached are: the flight-path angle, angle of attack, and airfoil geometry. The airfoil geometry alone is described by its camber and thickness distribution and each of these is usually described by a number of parameters. The authors [2] presented a comprehensive parametric study for ground effect on cambered plates by using an unsteady model they developed and verified earlier for zero-thickness airfoils [3]. Camber parameters such as position and location of maximum camber and camberline geometry (family) were varied systematically for various angles of attack and flight-path angles. As for the unsteady effect of thickness, it appears to be lacking in the literature. Even steady effects of thickness reported in the literature are very limited and appear to be conflicting. In the steady analysis, the flow is solved around an airfoil at a fixed height above the ground. Repeating this at various heights was thought to simulate ground effects for an airfoil approaching the ground. It has been shown by the authors [2, 3] and others [4] that the flow is inherently unsteady even if the airfoil moves with constant velocity in a straight line towards the ground plane. This is due to the continuous change in the airfoil bound circulation and the resulting shedding of vorticity into the wake as the ground is approached.

The main objective in the present paper is to investigate theoretically the effects of thickness of the airfoil on the changes in the aerodynamic coefficients as the airfoil approaches the ground. The model [3] developed previously to represent the unsteady nature of the problem for airfoils with zero thickness is extended to handle airfoils with thickness. Thickness effects are accounted for by using linear vortex distribution over surface elements (panels) similarly as in reference [5]. The developed model is verified and then used to quantify the effects of thickness parameters such as thickness ratio, position of maximum thickness and thickness profile shape on the deviations in C_l and C_m as the airfoil approaches the ground. These results are compared with those obtained by using the steady ground approach. The objective of this comparison is to show to what extent the results of the steady approach can be disastrous for a range of flight-path angles and angles of attack and in what range do they agree with those of the unsteady analysis. Identifying the range of such parameters in which this approach can be trusted is of great value because of its simplicity and extreme numerical efficiency compared to the unsteady analysis.

PREVIOUS WORK

The first study on ground effect dates back to 1922 when Wieselsberger [6] modeled such effect by placing the image of the real wing below the ground plane. He used the lifting-line theory of Prandtl for an elliptic wing and treated the flow as steady. The work on (steady) ground effects up to 1935 was summarized by Pistolesi [7]. This included the exact solution developed by Tomotika *et al.* [8] for steady flow past a flat plate above the

ground. This solution showed that C_l and C_m decrease slightly initially and then increase sharply as the ground is approached with small to moderate angles of attack. Using the conformal mapping technique, Green obtained the exact solution for a circular-arc airfoil in 1940 [9] and later for a thick airfoil in 1947 [10]; both moving steadily near the ground. By keeping only 3 terms in the series expansion of the lift he found that thickness and camber have opposite effects on the aerodynamic coefficients near ground and concluded that a flat plate may approximate a real airfoil as far as the ground effects are concerned. Again using conformal mapping, Tomotika *et al.* [11] studied the steady ground effect on the lift of a Joukowski-type airfoil in 1951 and on the lift and pitching moment of a circular-arc plate in the same year [12]. They found that effects of thickness and camber are additive near the ground in the sense that both reduce $\Delta C_l/C_{l\infty}$ below those of a flat plate. This contradicts Green's results [9,10]. However they reported some calculations, in which 5 terms of Green's expansion of the lift coefficient were used, showing that thickness always reduces the deviation in C_l near ground, in agreement with their results.

All of the above work dealt with steady ground effect as described in the introduction. Only recently, Chen and Schweikhard [4] solved the problem of a flat plate approaching the ground including the unsteady effects. However, their model has the shortcoming of assigning the wake trajectory along the flight path. Katz [13] used a vortex-lattice method to study the flow around wings, used in racing cars, near the ground. Chang [14] and Chang and Muirhead [15] studied delta wings in unsteady flow near the ground experimentally. Nuhait [16], Nuhait and Mook [17], and Mook and Nuhait [18] used the vortex-lattice method to study unsteady flow around finite wings moving near the ground. The wake positions and vorticity were computed as part of the solution. Kemmerly *et al.* [19] experimentally evaluated a moving-model technique for the measurement of unsteady ground effect. They simulated the sink rate by moving the model horizontally over an upwardly inclined ground board. Lee *et al.* [20] conducted tests on finite wings near ground in unsteady flow.

Nuhait and Zedan [2, 3] used a 2-D vortex-lattice method, allowing the wake to deform and roll up, to study the unsteady flows around flat and thin cambered plates approaching the ground. They found that camber and angle of attack effects work in the same direction. For small angles of attack or small camber ratios, they showed that the aerodynamic coefficients decrease first and then increase as the ground is approached. For large angles of attack or large camber ratios, the aerodynamic coefficients are always weakened by the ground effect. The relative deviations of C_l and C_m from corresponding values far from ground were found to decrease as the camber ratio or angle of attack increases. Based on this review, it appears that the unsteady effects of thickness of an airfoil approaching the ground have not been studied in the literature.

APPROACH

The flow is assumed to be 2-D and irrotational and the fluid to be incompressible and inviscid. The ground effect is simulated by placing an image of the real airfoil below the ground and thereby making the ground a plane of symmetry (Figure 1). The airfoil in the present model is rigid and it moves through the air which is otherwise still. The flight-path angle γ and the vertical speed of the airfoil (with respect to the ground) are related by $\gamma = \tan^{-1} -V_{AY}/V_{AX}$. In the present paper, the airfoil moves along a straight line (*i.e.* $\gamma = \text{constant}$). Three coordinate frames of reference are used. The first is fixed to the ground, the second is fixed to the airfoil (at the leading edge), and the third one is attached to each element (panel) on the airfoil surface. The ground and airfoil coordinate systems are shown in Figure 1 and the element coordinate system is shown later. In the following analysis all variables are made dimensionless by using the characteristic variables: speed of the airfoil U , physical length of the chord divided by half the number of elements L , ρU^2 for the pressure and L/U for the time.

The airfoil, its wake and their images are represented by sheets of vorticity. The bound vortex sheets representing the airfoil and its image have their positions specified. By placing the vortex sheets on the airfoil surface, thickness effects are accounted for and therefore there is no need to use source panels. The positions of the vortex

sheets representing the wake and its image are not known in advance. The wake rolls up and deforms into its force-free position. The vortex sheets representing the airfoil and its image are discretized into N elements ($N + 1$ nodes). The mid-point on each element is selected as the control point at which the no-penetration boundary condition is satisfied. The vorticity, which according to Kim [21], Kim and Mook [5], Dong [22], and Mook *et al.* [23] is equal to the surface velocity, is assumed to vary linearly along each element as shown in Figure 2. In order to make the calculations efficiently, a local coordinate system (x', y') for each element is used. This is the third frame of reference mentioned earlier. Some additional definitions are given in Figure 2.

The length of each element is normalized to unity for the purpose of computing the induced velocities (this is done locally in a subroutine). The vorticity $\bar{\gamma}$ over element j consists of two linear functions: $(G_{j+1})x'$ and $(G_j)(1 - x')$ as shown in Figure 3. In this figure, the two linear functions are referred to as Case 1 and Case 2. G_j and G_{j+1} are the unknown intensities of vorticity at nodes j and $j + 1$, respectively. The velocity components induced by the vorticity over element j at point $p(x'_p, y'_p)$ are given in the element frame of reference by the following formulas:

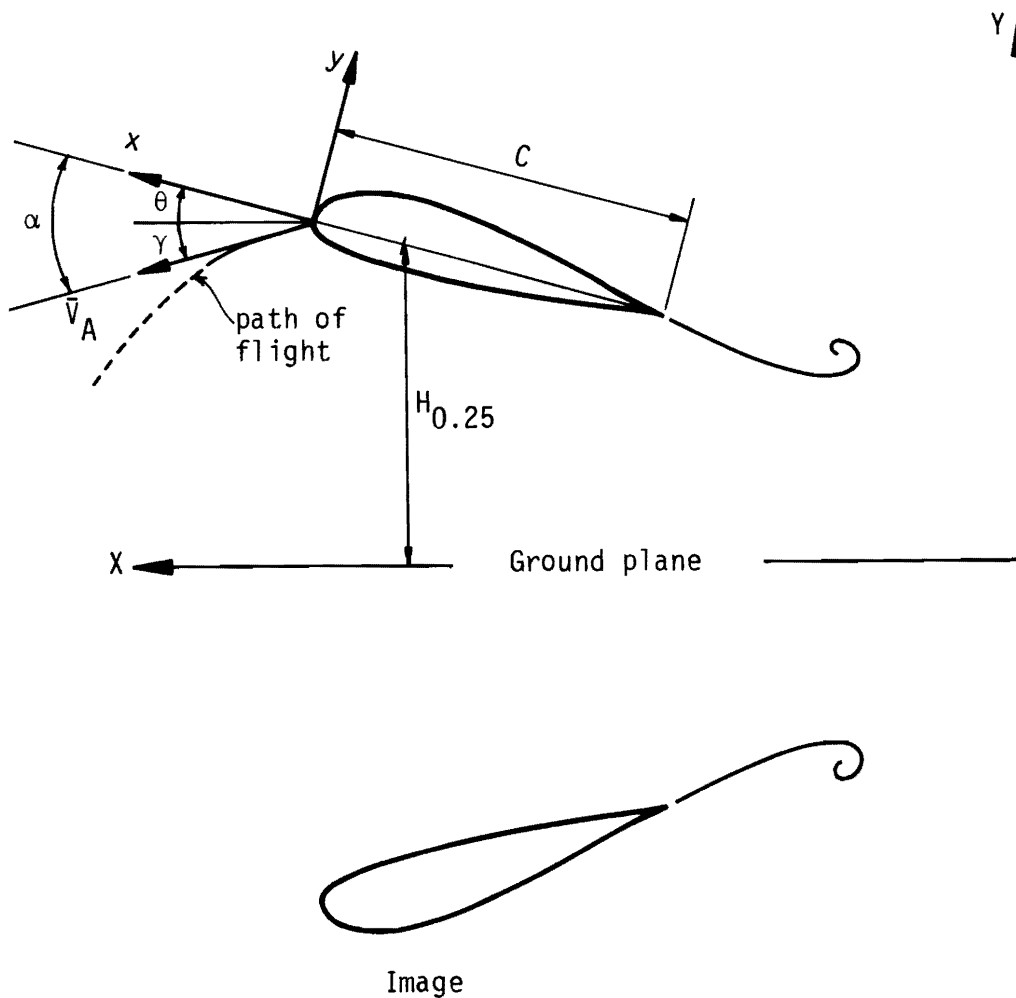


Figure 1. A Sketch of Airfoil and Its Image.

Case 1

$$\begin{aligned}
 V_{x'_{j+1,1}} &= \frac{G_{j+1}}{2\pi} \left[x'_p \Delta\theta + \frac{y'_p}{2} \ln R \right] \\
 V_{y'_{j+1,1}} &= \frac{G_{j+1}}{2\pi} \left[1 - y'_p \Delta\theta + \frac{x'_p}{2} \ln R \right]
 \end{aligned}
 \tag{1}$$

Case 2

$$\begin{aligned}
 V_{x'_{j,2}} &= \frac{G_j}{2\pi} \left[(1 - x'_p) \Delta\theta - \frac{y'_p}{2} \ln R \right] \\
 V_{y'_{j,2}} &= \frac{G_j}{2\pi} \left[\left(\frac{1 - x'_p}{2} \right) \ln R - 1 + y'_p \Delta\theta \right]
 \end{aligned}
 \tag{2}$$

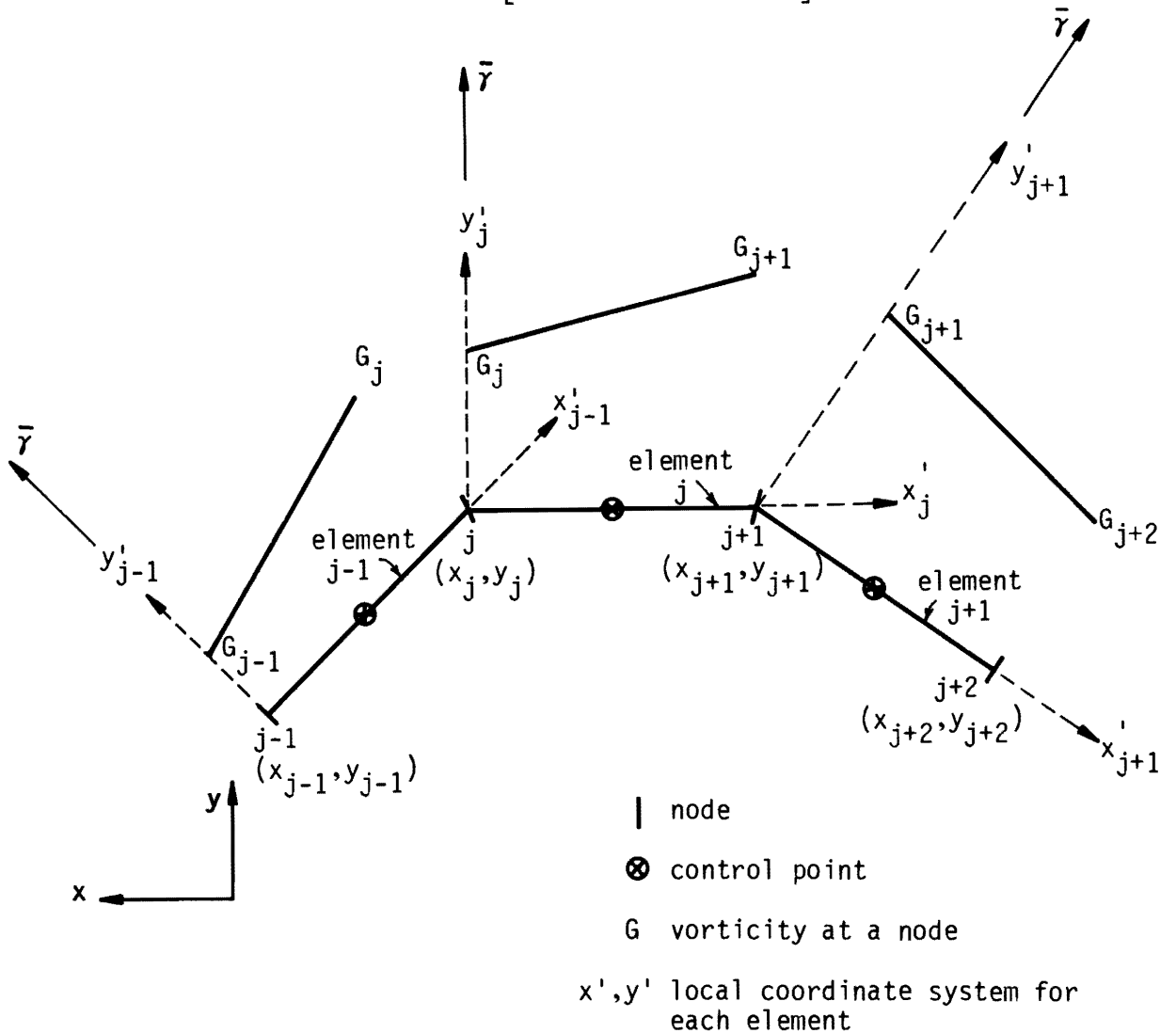


Figure 2. Vorticity Distribution Over Elements and Element Coordinate System.

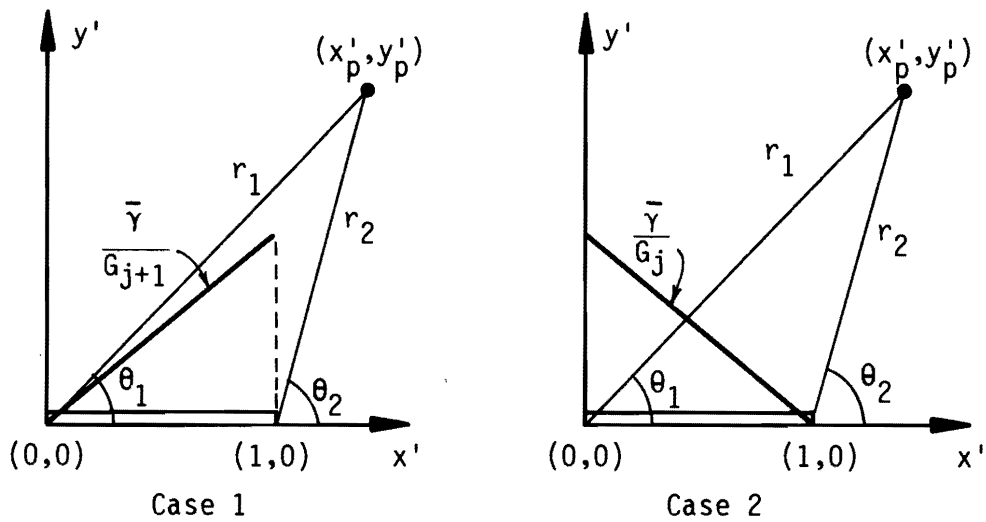


Figure 3. Splitting the Vorticity Distribution Over Element j Into Two Linear Functions.

where

$$\begin{aligned} \Delta\theta &= \theta_2 - \theta_1 \\ &= \tan^{-1}\left(\frac{x'_p}{y'_p}\right) - \tan^{-1}\left(\frac{x'_p - 1}{y'_p}\right) \\ R &= \left(\frac{r_2}{r_1}\right)^2 \\ &= \frac{(x'_p - 1)^2 + y'^2_p}{x'^2_p + y'^2_p} \end{aligned}$$

Subscripts j and $j + 1$ refer to the induced velocity contributions in terms of the vorticity at nodes j and $j + 1$, respectively. The subscripts 1 and 2 denote Case 1 and Case 2, respectively.

The velocity components in the body-fixed (x, y) frame of reference are given by:

$$\begin{Bmatrix} V_{x_{j+1,1}} \\ V_{y_{j+1,1}} \end{Bmatrix} = [T]^{-1} \begin{Bmatrix} V_{x'_{j+1,1}} \\ V_{y'_{j+1,1}} \end{Bmatrix} \tag{3}$$

for Case 1 and

$$\begin{Bmatrix} V_{x_{j,2}} \\ V_{y_{j,2}} \end{Bmatrix} = [T]^{-1} \begin{Bmatrix} V_{x'_{j,2}} \\ V_{y'_{j,2}} \end{Bmatrix} \tag{4}$$

for Case 2. The transformation matrix T is given by

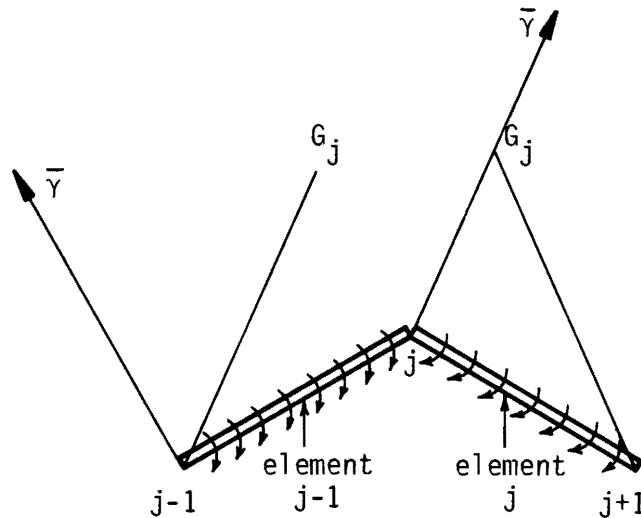


Figure 4. Vorticity Strength at Node j as it appears in Two Neighboring elements.

$$[T] = \frac{1}{\sqrt{(x_{j+1} - x_j)^2 + (y_{j+1} - y_j)^2}} \begin{bmatrix} (x_{j+1} - x_j) & (y_{j+1} - y_j) \\ (y_{j+1} - y_j) & -(x_{j+1} - x_j) \end{bmatrix} \quad (5)$$

in which x_j, y_j and x_{j+1}, y_{j+1} denote the coordinates of nodes j and $j + 1$ in terms of the body-fixed coordinates.

Equations (3) and (4) give the induced velocity at a point p by the vorticity over element j in terms of the vorticity at nodes j and $j+1$. The velocity induced at point p by unit-intensity vorticity at node j (vorticity over element $j-1$, case 1, plus vorticity over element j , case 2, see Figure 4) is given by

$$\mathbf{V}_j = \mathbf{V}_{j,1}/G_j + \mathbf{V}_{j,2}/G_j. \quad (6)$$

Point p is a general point in the flow field. In order to impose the no-penetration boundary condition, point p is selected at the control point of element i . The normal velocity at the control point i induced by the vorticity at node j (with unit intensity), A_{ij} , is equal to the normal velocity induced by the vorticity over element j (case 2) plus the normal velocity induced by the vorticity over element $j - 1$ (case 1) and their images, at control point i . That is

$$A_{ij} = \mathbf{V}_j \cdot \mathbf{n}_i \quad (7)$$

where \mathbf{n}_i is the unit vector normal to element i and \mathbf{V}_j is the velocity induced at control point i by the vorticity at node j and its image as given by Equation (6).

To simulate the unsteady flow, we follow Kim and Mook [5] and Mook *et al.*, [23] by placing a vortex core with a circulation Γ_c at the trailing edge. The normal velocity Q_i at control point i , induced by this vortex core (with a unit circulation) and its image, is given by

$$Q_i = (\mathbf{V}_{TE})_i \cdot \mathbf{n}_i \quad (8)$$

where $(\mathbf{V}_{TE})_i$ is the velocity induced at control point i by a vortex core with unit circulation at the trailing edge and its image.

The no-penetration boundary condition enforced at control point i on the airfoil is given by

$$\sum_{j=2}^N A_{ij} G_j - Q_i \Gamma_c = (\mathbf{V}_A - \mathbf{V}_W)_i \cdot \mathbf{n}_i \quad \text{for } i = 1, 2, \dots, N \quad (9)$$

\mathbf{V}_A is the airfoil velocity and \mathbf{V}_W is the velocity induced by the vortex cores in the wake and their images.

It follows from Kelvin's Theorem that the total circulation must be conserved (zero in this paper):

$$\frac{1}{2} \sum_{j=2}^N (l_{j-1} + l_j) G_j - \Gamma_c = \sum_{k=1}^{NT-1} \Gamma_{Wk} \quad (10)$$

where l denotes the length of the element. Γ_{Wk} is circulation of wake vortex core k . NT is the number of time steps the solution has advanced as discussed later.

Equations (9) and (10) form an overdetermined system of $N+1$ equations in N unknowns (G_2, G_3, \dots, G_N and Γ_c). We use the method of Lagrange multipliers to minimize the sum of the squares of errors of Equation (9) subject to the constraint of Equation (10) to obtain a solution of this system.

At the beginning of the first time step ($NT = 1$), \mathbf{V}_W is zero (no wake exists yet). The solution of the system of equations yields ($G_2, G_3, G_4, \dots, G_N$ and Γ_c). At the beginning of the second time step ($NT = 2$), the vortex core at the trailing edge (Γ_c) is shed at the local fluid particle velocity (in order to satisfy the so called unsteady Kutta condition [16]). Its circulation does not change to satisfy the temporal conservation of circulation. The new position of the vortex core (starting vortex) is computed by the Euler method using the following equation. Thus

$$\mathbf{r}(t + \Delta t) = \mathbf{r}(t) + \mathbf{v}(t) \Delta t \quad (11)$$

where $\mathbf{v}(t)$, the local fluid particle velocity at position $\mathbf{r}(t)$ at time t , is computed by using the following equation

$$\mathbf{v} = \mathbf{V} - \mathbf{V}_A \quad (12)$$

where \mathbf{V} is the absolute velocity induced by the bound and free vorticity and their images. The values of \mathbf{v} used in Equation (11) are those computed in the previous time step ($NT = 1$). Convecting this vortex core starts the generation of the wake.

The right-hand sides of Equations (9) and (10) are computed. The solution of the over-determined system of equations at the end of the second time step yields new values for $G_2, G_3, G_4, \dots, G_N$ and Γ_c . At the beginning of the third time step, the new vortex core at the trailing edge Γ_c is shed and the one from the start is convected downstream. This procedure can be repeated indefinitely. To start the procedure, one needs initial conditions. These are the position of the airfoil, pitch angle, flight-path angle, and wake positions and vorticity.

The aerodynamic forces and moments are computed by integrating the pressure distribution on the surface of the airfoil. The pressure on each element is given by the unsteady Bernoulli equation:

$$\frac{\partial \Phi}{\partial t} + \frac{1}{2} \mathbf{V} \cdot \mathbf{V} + P = P_\infty \quad (13)$$

where Φ is the velocity potential in ground-fixed coordinates, and P and P_∞ are the dimensionless pressures on airfoil surface and at infinity, respectively. It is more convenient, in the present problem, to apply Bernoulli's equation with respect to the moving coordinate system. Denoting the velocity potential in the moving coordinate system by ϕ , one can show that (Karamcheti [24]) $\partial \Phi / \partial t = \partial \phi / \partial t - \mathbf{V} \cdot \mathbf{V}_A$. Thus, Equation (13) becomes

$$\frac{\partial \phi}{\partial t} - \mathbf{V} \cdot (\mathbf{V}_A - \frac{\mathbf{V}}{2}) + P = P_\infty \quad (14)$$

The pressure coefficient at a control point i is given by

$$\begin{aligned} C_{p_i} &= 2(P_i - P_\infty) \\ &= -2 \left. \frac{\partial \phi}{\partial t} \right|_i - \mathbf{V}_i \cdot (\mathbf{V} - 2\mathbf{V}_A)_i \end{aligned} \quad (15)$$

\mathbf{V}_i is the absolute velocity at control point i which is induced by the bound and the wake vorticity and their images. $\partial \phi / \partial t$ at control point i is approximated by the following finite-difference expression:

$$\left. \frac{\partial \phi}{\partial t} \right|_i \simeq \frac{\phi_i(t + \Delta t) - \phi_i(t)}{\Delta t} \quad (16)$$

The values of all ϕ_i for two successive time steps are stored. The value of ϕ_i at the current time level is obtained by numerically evaluating the line integral,

$$\phi_i = \phi_{i-1} + \int_{S_{i-1}}^{S_i} \mathbf{V} \cdot d\mathbf{S} \quad (17)$$

where \mathbf{V} is the particle velocity and \mathbf{S} represents the integration path. For control point 1, Equation (17) reduces to

$$\phi_1 = \phi_0 + \int_{S_0}^{S_1} \mathbf{V} \cdot d\mathbf{S} \quad (18)$$

where "0" represents some reference point. In order to compute ϕ_1 , one has to know ϕ_0 at each time step. In the present paper, point 0 was selected to be very far (200 chords) in front of the airfoil. This was verified to be too far to be affected by the airfoil motion at any time level even when the airfoil reaches the ground. The value of ϕ_0 was chosen to be zero (impulsive start). The chosen path between point 0 and control point 1 consists of two straight lines. One line is vertical and the other is horizontal. The integral term in Equation (18) is approximated by using the trapezoidal rule with unequal steps. The number of integration steps were chosen to be 20 in the vertical direction and 100 in the horizontal direction. Once ϕ_1 is computed at a given time level, the values of ϕ at other control points can be evaluated by the recurrence integral relation of Equation (17). The results were checked by allowing the solution to reach steady state and comparing it with known exact steady results as discussed below.

CALIBRATION OF THE METHOD

The method described in the previous section was programmed and run on an IBM- 370 8083 JX mainframe computer. To save computer time the earlier shed vortex cores are ignored once the number of cores in the wake reaches a certain number N_{core} . To determine appropriate values for N_{core} , the number of elements

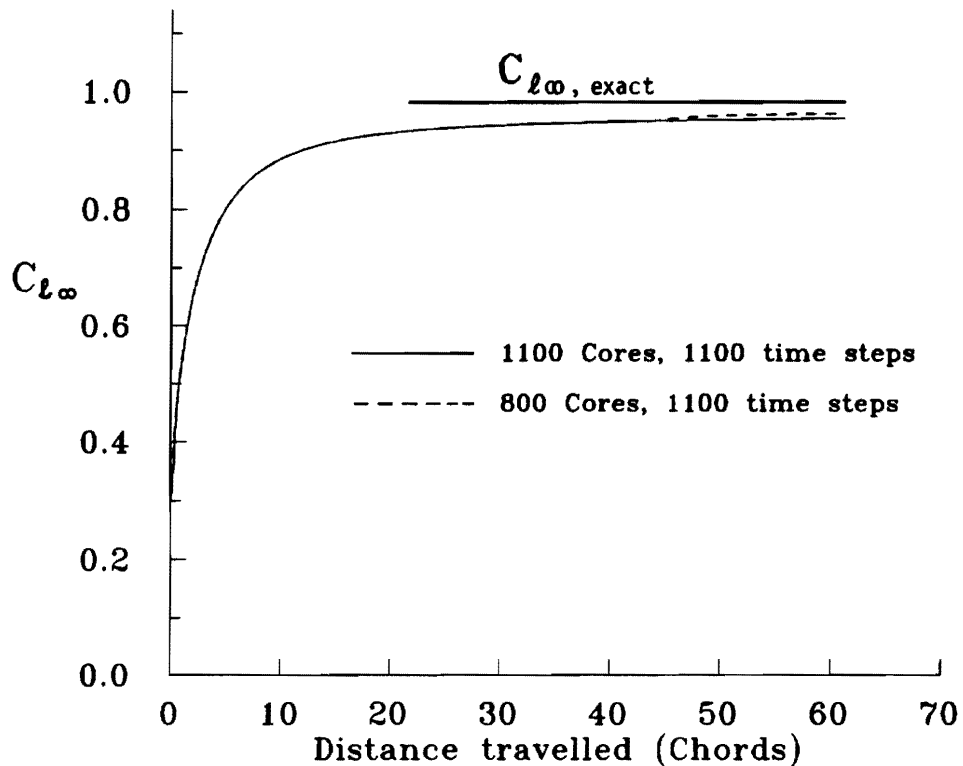


Figure 5. The Variation of Lift Coefficient of NACA 0012 Airfoil Far from Ground with Distance Traveled as Computed by the Model at $\alpha = 8.3^\circ$.

N and the time step Δt , a limited sensitivity study was made. In this study N_{core} , N and Δt were varied systematically by varying one parameter at a time while fixing the other two. The test case used is a NACA 0012 airfoil impulsively started very far from ground with $\alpha = 8.3^\circ$. The solution is continued until steady flow is established. The computed lift coefficient C_l increases with time until it reaches an asymptotic value. Comparing this value with the exact steady lift coefficient (which is 1.0 for $\alpha = 8.3^\circ$) [25] is used as a criterion to judge the accuracy of the solution. The values of the parameters investigated are: $N_{core} = 800$ and 1100, $N = 36, 60$ and 72 and $\Delta t = 1, 2$, and 3. With 1100 times steps, all combinations of parameters gave small errors in general. A combination of $N_{core} = 800, N = 72$ and $\Delta t = 2$ gave reasonably accurate results. In fact such a combination presented a good compromise between accuracy and computing time. The latter is quite important because unsteady calculations are time consuming. Figure 5 shows the variation of C_l versus time for this combination of model parameters once with truncation at $N_{core} = 800$ and another time without truncation. A negligibly small jump is noticed at the time corresponding to when truncation occurred. The asymptotic value is very close to the exact $C_l (= 1.0)$ in both cases. The unsteady results presented from this point on were obtained by using these solution parameters.

We found no results for the unsteady ground effect for thick airfoils in the literature to compare with. Therefore, the present (unsteady) model was verified near the ground by comparing the asymptotic values of $\Delta C_l / C_{l\infty}$ with the corresponding results of a steady-flow vortex-panel method that accounts for ground effects. In the steady method, the system of over determined equations (9) with $\mathbf{V}_w = 0$ (no wake) and $Q_i = 0$ (no starting vortex) is solved for G_i by using a least-square-error method. The steady Kutta condition ($\bar{\gamma}_{T.E} = 0$) is implicitly satisfied in this system ($G_1 = G_{N+1} = 0$). Table 1 gives such a comparison for a NACA 0024 airfoil with $\alpha = 6^\circ$ and $\gamma = 0^\circ$, at $h_{0.25} = 0.25$ and 0.375. The results indicate that the method works very well. The deviations in C_l and C_m are defined as

$$\begin{aligned} \Delta C_l / C_{l\infty} &= (C_l - C_{l\infty}) / C_{l\infty} \\ \Delta C_m / C_{m\infty} &= (C_m - C_{m\infty}) / C_{m\infty} \end{aligned}$$

and $h_{0.25}$ is defined as the height of the 1/4-chord point above the ground normalized by the chord.

Table 1. Comparison Between Asymptotic Values of $\Delta C_l / C_{l\infty}$ and $\Delta C_m / C_{m\infty}$ with Values Obtained from Steady Ground Effect program

$h_{0.25}$	Unsteady ground effect (asymptotic values)			Steady ground effect		
	$\Delta C_l / C_{l\infty}$	$\Delta C_m / C_{m\infty}$	$\Delta \Gamma / \Gamma_\infty$	$\Delta C_l / C_{l\infty}$	$\Delta C_m / C_{m\infty}$	$\Delta \Gamma / \Gamma_\infty$
0.25	-0.14151	-0.27721	-0.06874	-0.14145	-0.27709	-0.06867
0.375	-0.00205	-0.01581	0.04066	-0.00201	-0.01561	0.04071

RESULTS AND DISCUSSION

The effects of thickness on the deviations in the aerodynamic parameters $\Delta C_l/C_{l\infty}$ and $\Delta C_m/C_{m\infty}$ as the airfoil approaches ground are investigated systematically by using both the steady and unsteady approaches described earlier. The thickness parameters whose effect is investigated are: the thickness ratio τ , the position of maximum thickness m and the shape of the thickness profile.

Results of Steady Ground Effect

Figure 6a shows the deviation in the lift coefficient versus the height of the 1/4-chord point for symmetric airfoils (camber ratio $e = 0$) moving steadily parallel to the ground ($\gamma = 0^\circ$) with $\alpha = 6^\circ$. These NACA 4-digit airfoils have different thickness ratios. We observe that the effect of thickness on the deviation is limited to

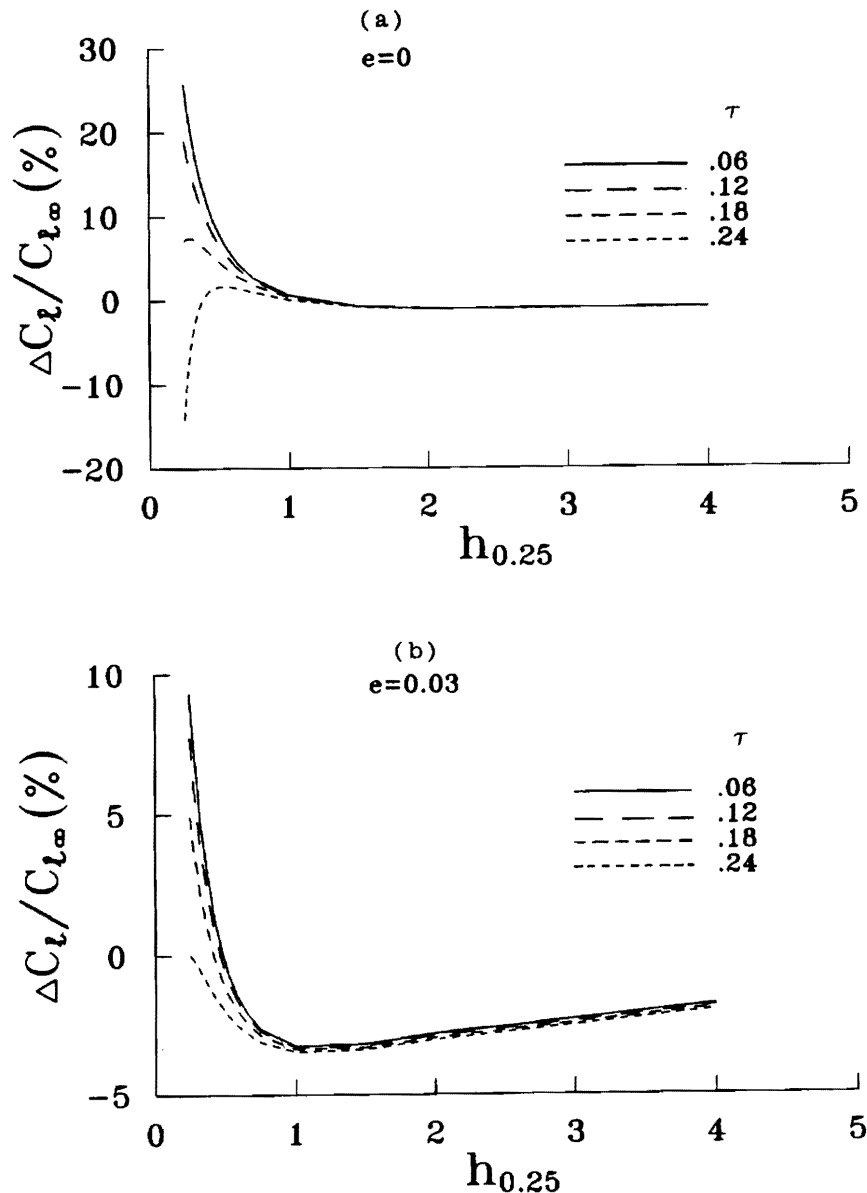


Figure 6. Effect of Thickness Ratio on Deviations in C_l of Symmetric (top) and Cambered (bottom) NACA 4-Digit Series Airfoils in Steady Ground Effect ($\gamma = 0^\circ$) at $\alpha = 6^\circ$.

$h_{0.25} < 1.0$ where increasing the thickness ratio tends to reduce $\Delta C_l/C_{l\infty}$ as the ground is approached. It is interesting to note that this reduction increases very fast with τ to the point of giving negative deviation (C_l is below $C_{l\infty}$) very close to the ground for $\tau = 0.24$. This may be attributed to the constriction of the flow (Venturi effect) which causes a reduction in the pressure on the lower surface of the airfoil resulting in lower C_l . This effect appears to dominate over the effect of the airfoil image for this extreme thickness ratio very close to the ground.

The investigation was repeated for cambered airfoils with $e = 0.03$ as shown in Figure 6b. The trends are similar to those observed in Figure 6a, however for the same thickness ratio, the magnitudes of $\Delta C_l/C_{l\infty}$ are lower because of the effect of the 3% camber which causes further reduction as expected [11,12]. An exception to that is the results for $\tau = 0.24$ very close to the ground where the cambered airfoil gives higher $\Delta C_l/C_{l\infty}$ than the case with zero camber. We attribute this behavior to the fact that adding camber eases the constriction of

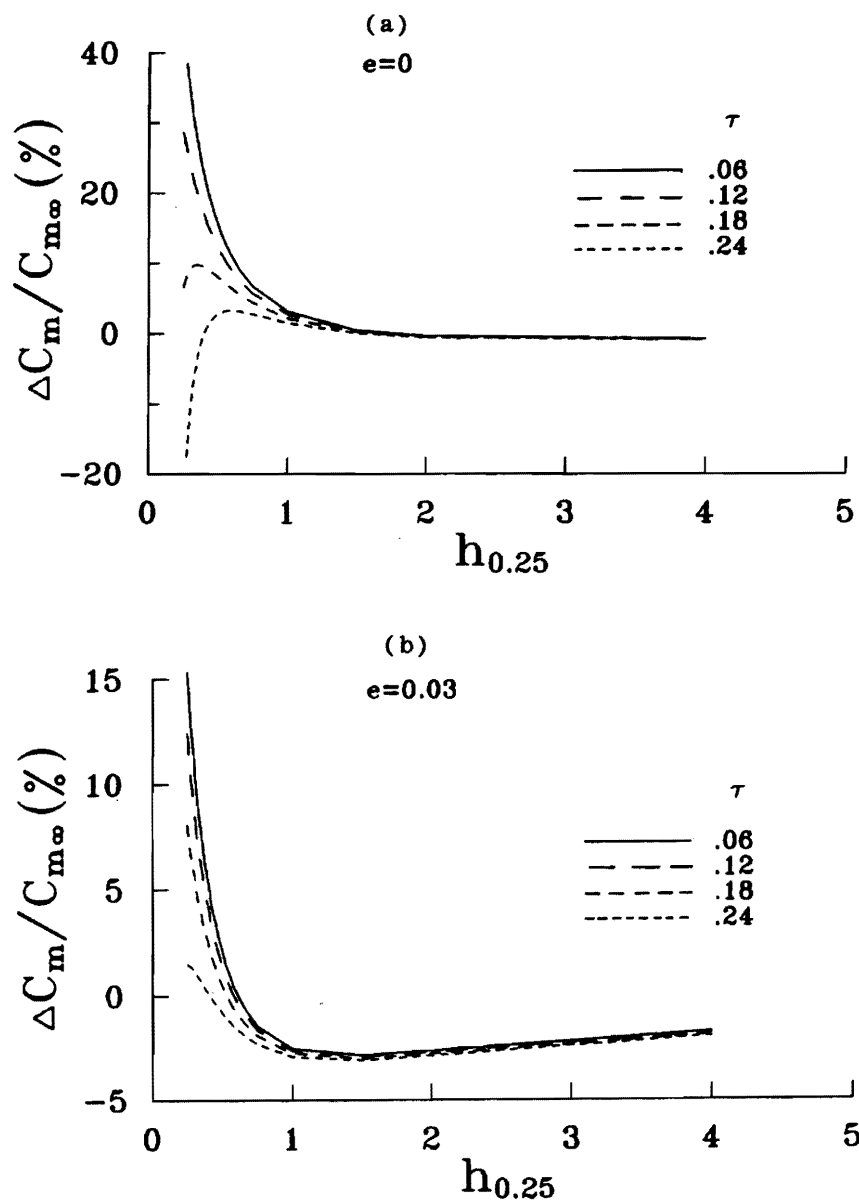


Figure 7. Effect of Thickness Ratio on Deviations in C_m of Symmetric (top) and Cambered (bottom) NACA 4-Digit Series Airfoils in Steady Ground Effect ($\gamma = 0^\circ$) at $\alpha = 6^\circ$.

the flow between the airfoil and the ground for such a large τ . Increasing the camber further causes the effects of τ to decrease quite fast. Figure 7 shows the deviation in the moment coefficient for same airfoils used in Figure 6. The trends are similar to those observed for $\Delta C_l/C_{l\infty}$; however the magnitude of the deviations are generally bigger.

The effect of the location of maximum thickness m on $\Delta C_l/C_{l\infty}$ and $\Delta C_m/C_{m\infty}$ was investigated for $\tau = 0.12$ at $\alpha = 6^\circ$ by using the modified NACA 4-digit series airfoils [25]. Although m was varied over a wide range (0.2 to 0.6), the effect was negligible for symmetric ($e = 0$) and cambered airfoils ($e = 0.03$) as shown in Figure 8. Again the deviation in the moment coefficient is larger than the deviation in the lift coefficient. The effect of the shape of thickness profile was investigated by comparing $\Delta C_l/C_{l\infty}$ and $\Delta C_m/C_{m\infty}$ for a symmetric NACA 4-digit series airfoil with $\tau = 0.18$ and $m = 0.3$ with those for a symmetric Karman-Trefftz airfoil with the same τ and m ; both at $\alpha = 6^\circ$. The results of the comparison, which are shown in Figure 9, indicate negligible effect.

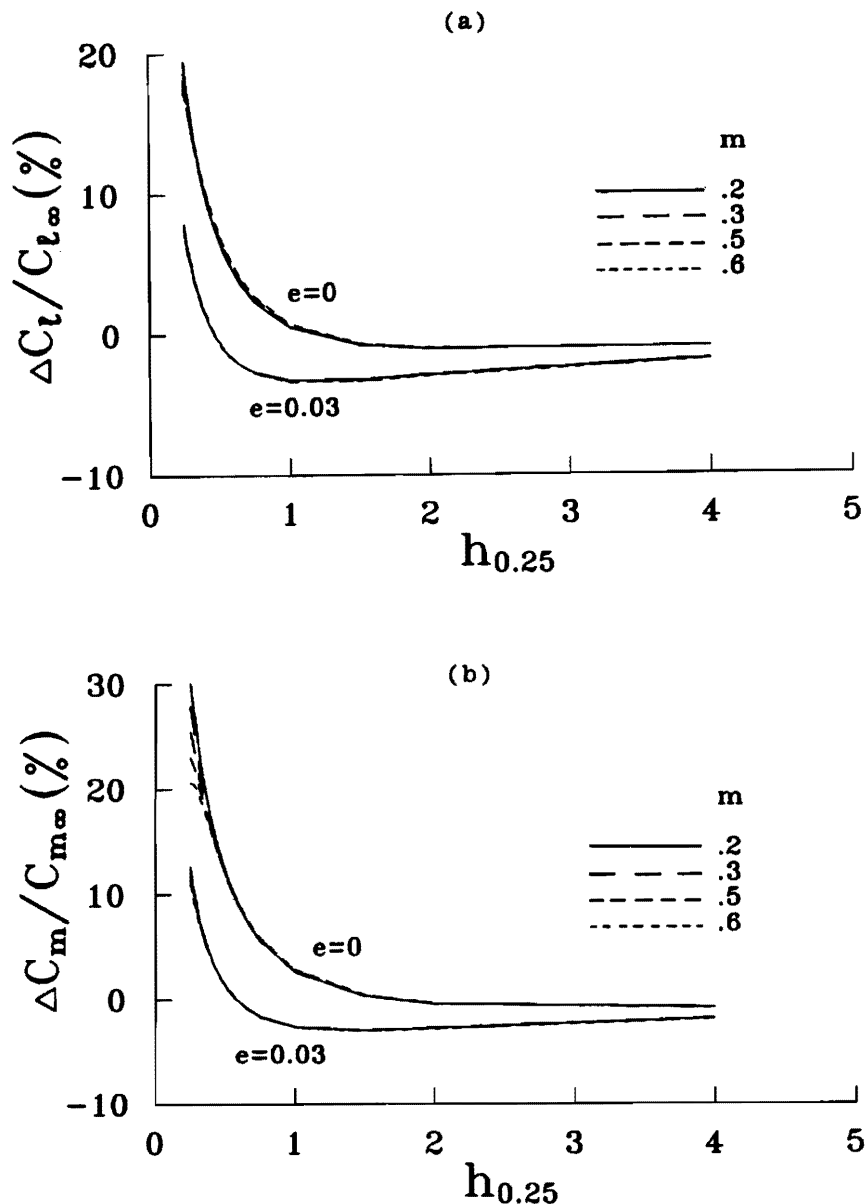


Figure 8. Effect of Position of Maximum Thickness on Deviations in C_l and C_m of Symmetric and Cambered NACA 4-Digit Series (Modified) Airfoils with $\tau = 0.12$ in Steady Ground Effect ($\gamma = 0^\circ$) at $\alpha = 6^\circ$.

Results of Unsteady Ground Effect

The unsteady model was used to study the effects of the thickness parameters considered above. In these investigations the airfoil is impulsively started with the appropriate values of γ and α far enough from the ground to allow reaching steady flow before ground effects become noticeable as done in reference [3].

Fixing γ at 30° and α at 6° , the effects of τ on $\Delta C_l/C_{l\infty}$ and $\Delta C_m/C_{m\infty}$ were investigated for symmetric and cambered NACA 4-digit series airfoils. The results of this investigation are shown in Figure 10. It seems very surprising that the effect of τ , on the deviations in C_l is negligible for both camber ratios and is generally small on the deviation in C_m for $e = 0$ and negligible for $e = 0.03$. This appears to be in clear conflict with the results of the steady analysis presented earlier. Figure 11a shows that the effect of the location of maximum thickness on $\Delta C_l/C_{l\infty}$ is generally small. The corresponding results in Figure 11b indicate that $\Delta C_m/C_{m\infty}$ is slightly reduced as the maximum thickness is moved towards the trailing edge for both symmetric and cambered ($e = 0.03$) airfoils. The effect of thickness distribution (profile shape) is studied by comparing $\Delta C_l/C_{l\infty}$ and

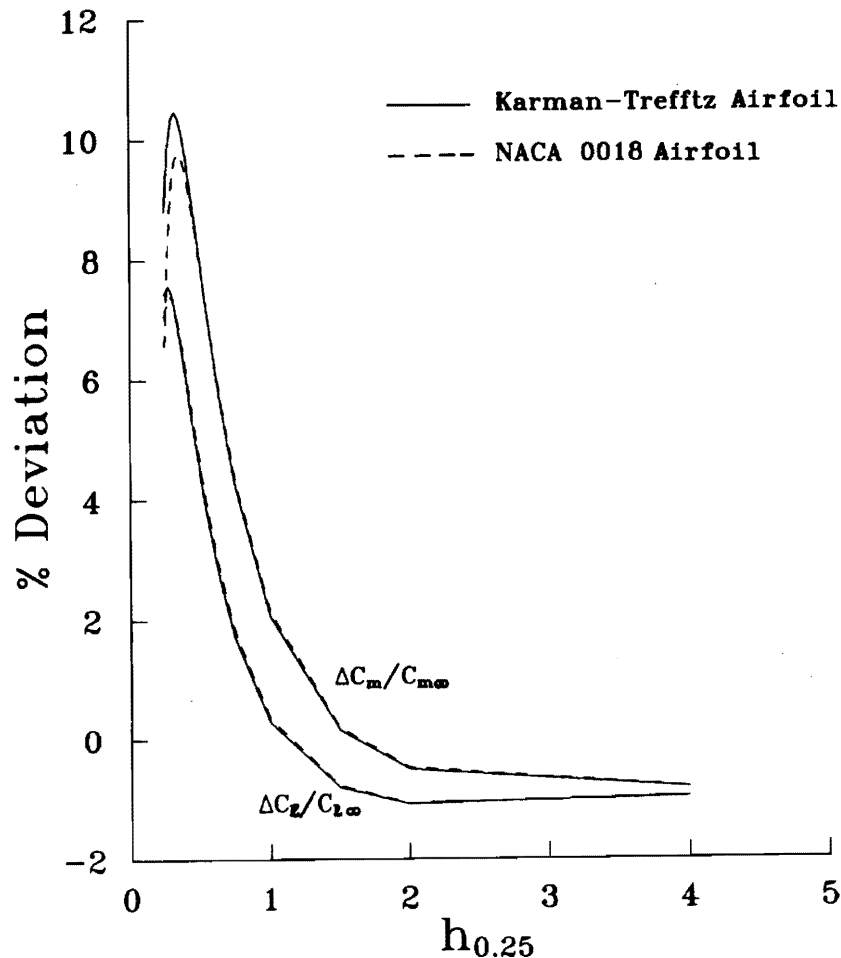


Figure 9. Comparison of Deviations in C_l and C_m for Symmetric Karman-Trefftz and NACA 4-Digit Series Airfoils with $\tau = 0.18$ and $m = 0.3$ in Steady Ground Effect ($\gamma = 0^\circ$) at $\alpha = 6^\circ$.

$\Delta C_m/C_{m\infty}$ for a Karman-Trefftz airfoil and the NACA 0018 airfoil; both airfoils are symmetric with $\tau = 0.18$ and $m = 0.3$. The results shown in Figure 12 indicate that the two profiles have essentially the same $\Delta C_l/C_{l\infty}$; however the Karman-Trefftz airfoil has a slightly higher $\Delta C_m/C_{m\infty}$.

The apparent contradiction between the steady and unsteady effects of τ indicates that the effect of γ (or θ) may be the key to explain it. Therefore it was decided to add the effect of γ for a given airfoil to the original

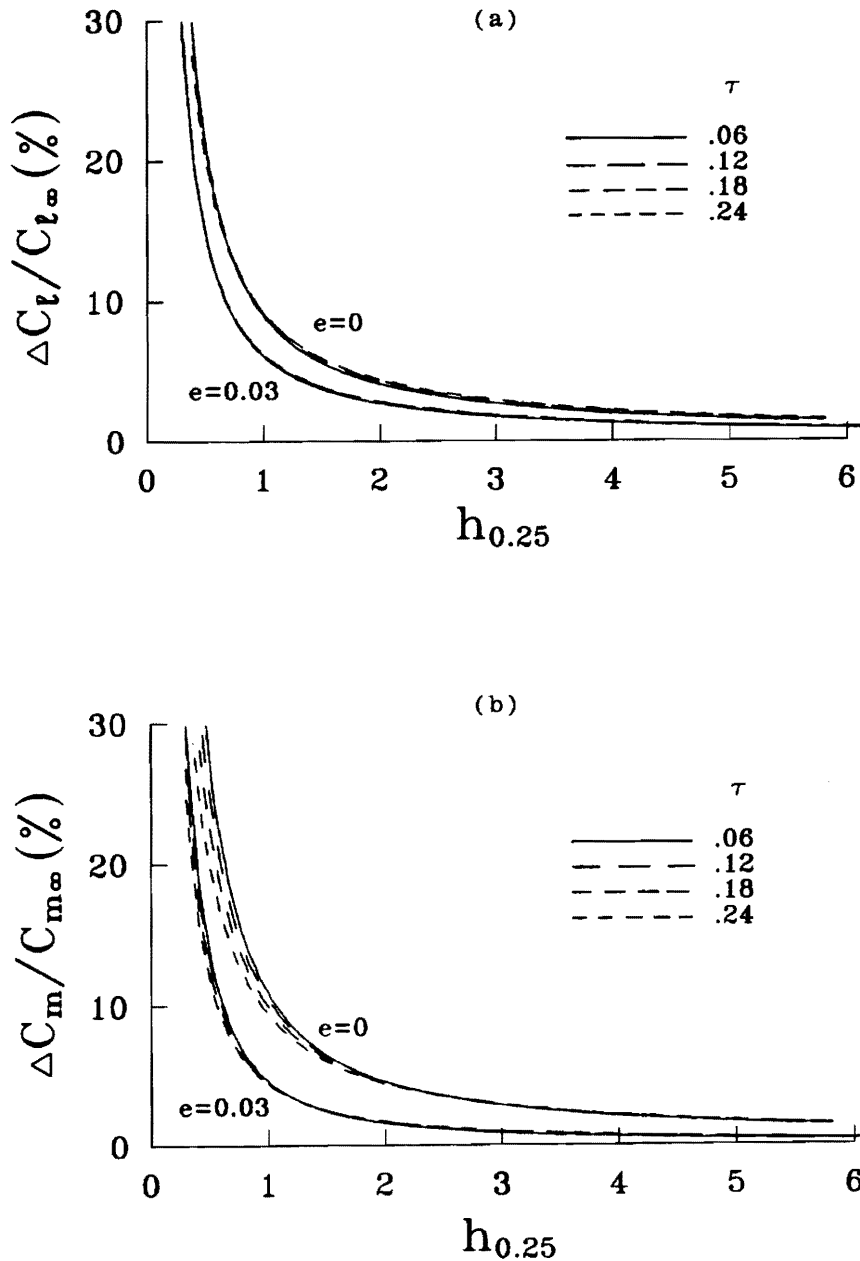


Figure 10. Effect of Thickness Ratio on Deviations in C_l and C_m of Symmetric and Cambered NACA 4-Digit Series Airfoils in Unsteady Ground Effect; $\gamma = 30^\circ$ and $\alpha = 60^\circ$.

investigation. We investigated two symmetric NACA 4-digit series airfoils with $\tau = 0.24$ and 0.12 at $\alpha = 6^\circ$. The variation of $\Delta C_l/C_{l_\infty}$ for the NACA 0024 airfoil is shown in Figure 13a, at $\gamma = 50^\circ, 30^\circ, 10^\circ, 5^\circ$ and 2° in addition to the steady results ($\gamma = 0^\circ$). The values of the pitch angle θ corresponding to these values of γ are given on the figure. The corresponding results for the NACA 0012 airfoil are shown in Figure 13b. As expected, the effect of γ is quite substantial and shows a clear trend. Reducing γ , decreases $\Delta C_l/C_{l_\infty}$ for both values of τ . Further it is noted that the reversal of the sign of $\Delta C_l/C_{l_\infty}$ near ground for $\tau = 0.24$ is not limited to the

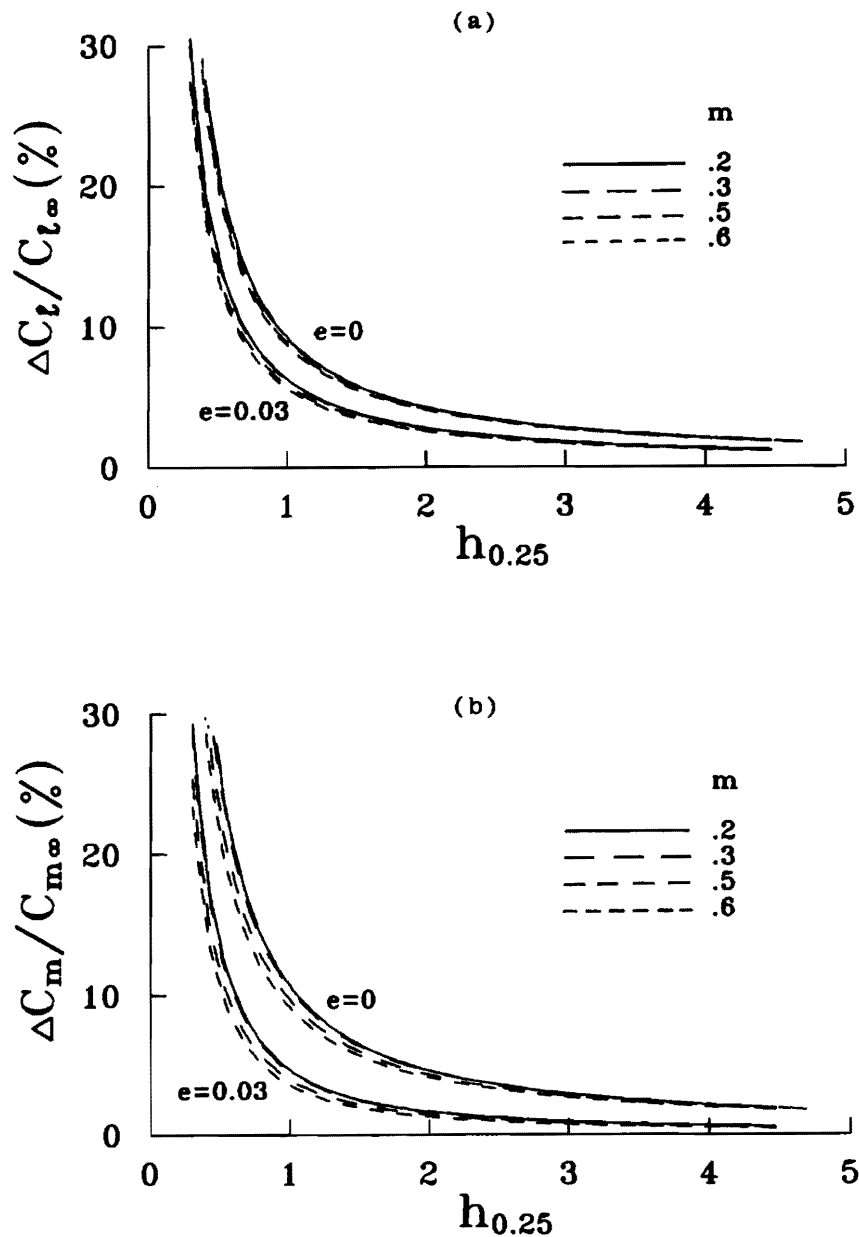


Figure 11. Effect of Position of Maximum Thickness on Deviations in C_l and C_m of Symmetric and Cambered NACA 4-Digit Series Airfoils in Unsteady Ground Effect; $\gamma = 30^\circ$ and $\alpha = 6^\circ$.

steady case ($\gamma = 0$); in fact it appears at $\gamma = 2^\circ$ and 5° ($\theta = 4^\circ$ and 1°). Since θ is positive (airfoil nose is higher than its trailing edge) in these three cases only at $6^\circ, 4^\circ$ and 1° , it appears that the constriction of the flow between the airfoil and the ground, is the reason for the drop in the aerodynamic coefficients very close to the ground. To test this hypothesis, the pressure distribution on the NACA 0024 airfoil when it is located at $h_{0.25} = 0.25$, as it moves towards ground with $\gamma = 30^\circ, 5^\circ$ and 2° , is plotted in Figure 14. The pressure distribution

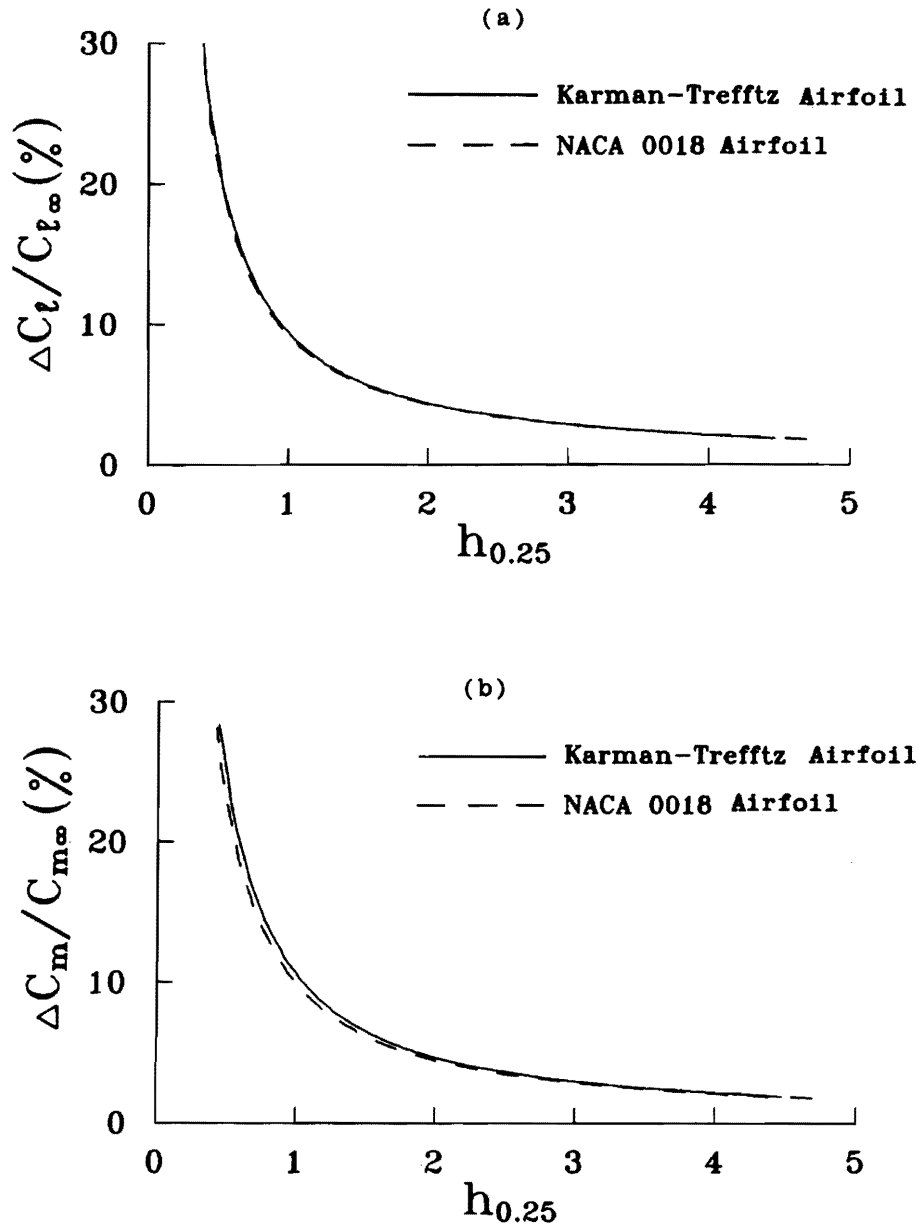


Figure 12. Comparison of Deviations in C_i and C_m for Symmetric Karman-Trefftz and NACA 4-Digit Series Airfoils with $\tau = 0.18$ and $m = 0.3$ in Unsteady Ground Effect; $\gamma = 30^\circ$ and $\gamma = 6^\circ$.

obtained from the steady analysis ($\gamma = 0$) with the airfoil at the same height is also shown on the same figure. The results indicate a reduction in the pressure on the lower surface of the airfoil as γ decreases with the lowest pressure given by the steady analysis ($\gamma = 0^\circ$). For values of $\gamma \leq 5^\circ$ ($\theta \geq 1^\circ$) the pressure becomes lower than the freestream value causing suction in a region on the airfoil's lower surface; the extent of this region increases as γ decreases. The presence of this suction region is responsible for the reduction in C_l very close to ground.

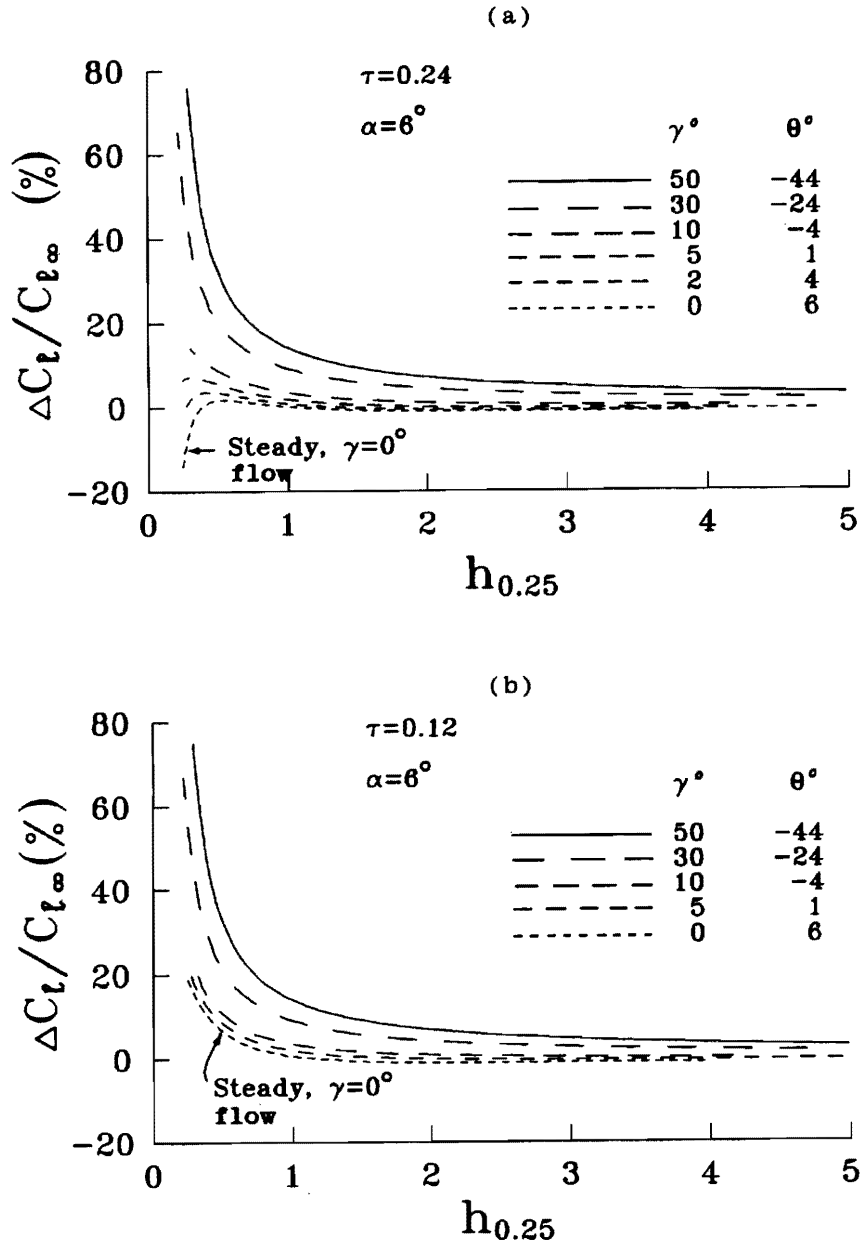


Figure 13. Effect of Flight Path Angle on Relative Deviation in C_l for NACA 0024 and NACA 0012 Airfoils in Unsteady Ground Effect; $\alpha = 6^\circ$

Limited results on the effect of thickness ratio on $\Delta C_l/C_{l\infty}$ at various γ (or θ) are extracted from Figures 13a and 13b and plotted in Figure 15. The results indicate almost no effect at $\gamma = 30^\circ$ ($\theta = -24^\circ$), very little effect at $\gamma = 10^\circ$ ($\theta = -4^\circ$) and clear effect especially close to the ground at $\gamma = 5^\circ$ ($\theta = 1^\circ$). For these last two values of γ , $\Delta C_l/C_{l\infty}$ is lower for $\tau = 0.24$ than for $\tau = 0.12$. To investigate this further we examine the pressure distributions. Figure 16a shows the pressure distribution over the thicker airfoil ($\tau = 0.24$) at $h_{0.25} = 0.5, 0.375$ and 0.25 for $\gamma = 5^\circ$. These results indicate that the extent of the suction region grows as the ground is approached. The corresponding results for the thinner airfoil ($\tau = 0.12$) with the same γ at the same α are shown in Figure 16b. We observe that the pressure on the lower surface increases as the ground is approached which explains the reason for the sharp increase of C_l near ground for thin airfoils.

SUMMARY AND CONCLUDING REMARKS

A model based on the image technique developed previously to compute the unsteady incompressible potential flow around cambered plates moving near ground is extended to handle airfoils with thickness. The model has been verified by comparing the computed asymptotic aerodynamic parameters for an impulsively started airfoil out of ground effect with the known exact steady parameters. The effects of airfoil thickness on the relative deviations in the lift and moment coefficients (from steady values out of ground effect), as the ground is approached, are studied by using this model. Airfoil thickness parameters whose effect is investigated are thickness ratio, location of maximum thickness and thickness profile shape. These parameters were varied one

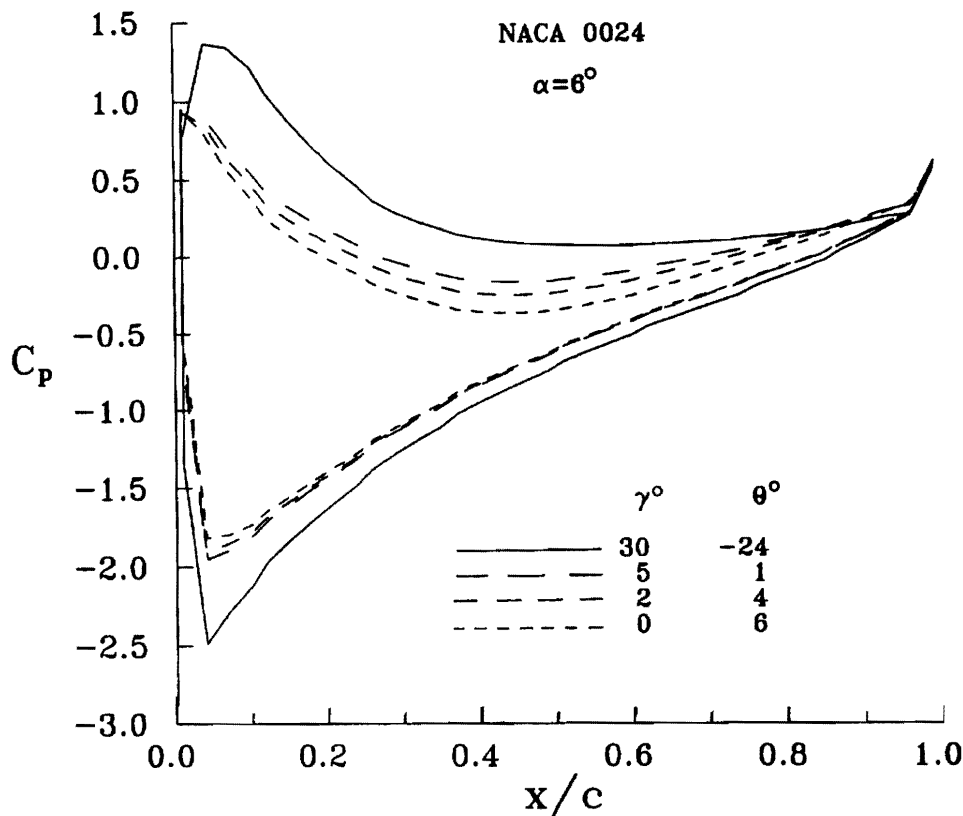


Figure 14. Pressure Distribution on the NACA 0024 in Unsteady Ground Effect at $h_{0.25} = 0.25$ for Different Flight Path Angles.

at a time. The investigation was conducted for symmetric airfoils and for airfoils with 0.03 camber ratio. The whole investigation was also repeated by using the steady analysis approach ($\gamma = 0$). The results of the steady approach are compared with those of the unsteady approach to identify the range of flight parameters in which the steady approach can be trusted and the range in which they are in big error.

The results indicate that the effects of thickness on $\Delta C_l/C_{l\infty}$ are negligible and are generally small on $\Delta C_m/C_{m\infty}$, when the airfoil nose is lower than its trailing edge (*i.e.* for combinations of flight path angles γ and angles of attack α giving negative pitch angle θ). As the value of θ increases above zero, both $\Delta C_l/C_{l\infty}$ and $\Delta C_m/C_{m\infty}$ drop with increasing thickness ratio. In fact with $\theta > 0^\circ$, $\Delta C_l/C_{l\infty}$ and $\Delta C_m/C_{m\infty}$ become negative near the ground for very high thickness ratios. This is attributed to the constriction of the flow between the ground and the airfoil which results in a reduction of the pressure over the lower surface of the airfoil. This may explain the apparent contradiction between the results of the steady approach, which showed substantial effects for the thickness ratio, and the results of the unsteady approach, which showed small effects, as a consequence to the differences in the pitch angle. Of course more work needs to be done to show that the effect of thickness on the deviations in the aerodynamic coefficients depends on the pitch angle mainly.

ACKNOWLEDGEMENT

The authors wish to thank the staff of King Saud University Computer Center for their cooperation and help.

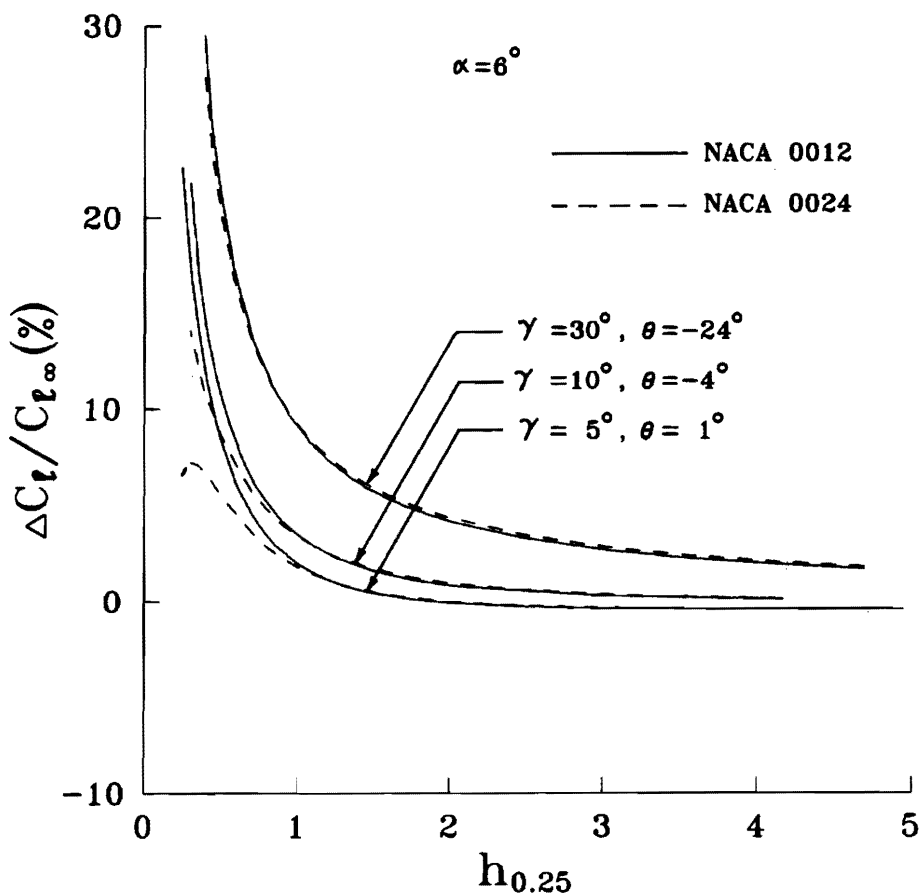


Figure 15. Unsteady Deviation in the Lift Coefficients of Two-Symmetric NACA Airfoils Approaching Ground with Different-Flight Path Angles at $\alpha = 6^\circ$.

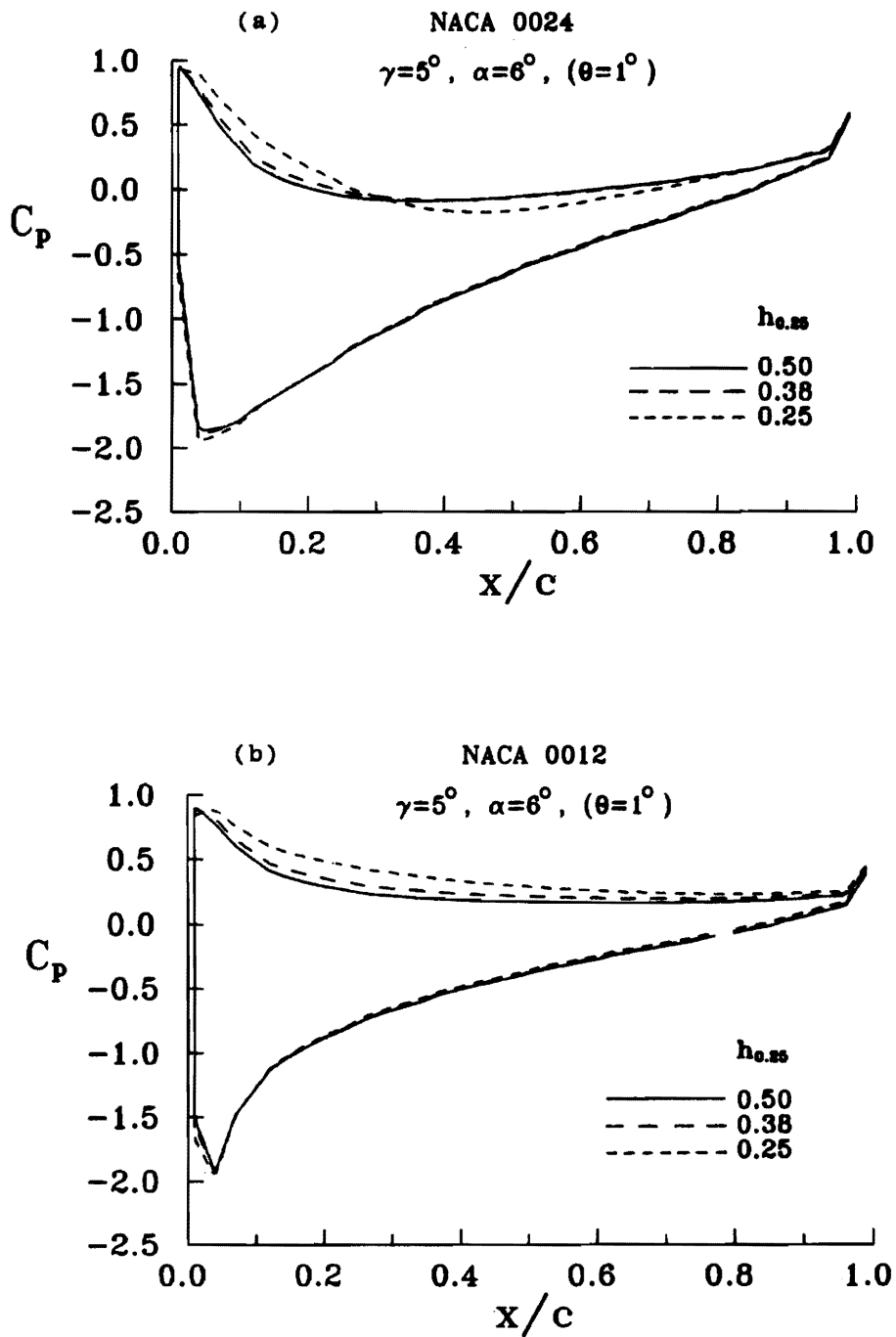


Figure 16. Pressure Distribution Over Airfoils at Various Heights Above Ground in Unsteady Ground Effect.

REFERENCES

- [1] A. H. Nayfeh, Private Communication, Feb. 1993.
- [2] M. F. Zedan and A. O. Nuhait, "Unsteady Effects of Camber on the Aerodynamic Characteristics of a Thin-Airfoil Moving Near Ground", *Aeronautical Journal of the Royal Aeronautical Society*, **96(959)** Nov. 1992, pp. 343-350.
- [3] A. O. Nuhait and M. F. Zedan, "Numerical Simulation of Unsteady Flow Induced by a Flat Plate Moving Near Ground", *Journal of Aircraft*, **30(5)** (1993), pp. 611-617.
- [4] Y.-S. Chen, and W. G. Schweikhard, "Dynamic Ground Effects on a Two-Dimensional Flat Plate", *Journal of Aircraft*, **22** July 1985, pp. 638-640.
- [5] M. J. Kim and D. T. Mook, "Application of Continuous Vorticity Panels to General Unsteady Incompressible Two-Dimensional Lifting Flows", *Journal of Aircraft*, **23** June 1986, pp. 464-471.
- [6] C. Wieselsberger, "Wing Resistance Near the Ground", *NACA TM 77*, 1922.
- [7] E. Pistolesi, "Ground Effect-Theory and Practice," *NACA TM 828*, 1935.
- [8] S. Tomotika, T. Nagamiya, and Y. Takenouti, "The Lift on a Flat Plate Placed Near a Plane Wall, with Special Reference to the Effect of the Ground Upon the Lift of a Monoplane Aerofoil," *Aeron. Res. Inst., Tokyo Imperial Univ. Report No. 97, Aug. 1933* (as reported in Pistolesi [7]).
- [9] A. E. Green, "The Forces Acting on a Circular-Arc Aerofoil in a Stream Bounded by a Plane Wall", *Proceedings London Mathematical Society*, **46** 1940, pp. 19-54.
- [10] A. E. Green, "The Two-Dimensional Aerofoil in a Bounded Stream", *Quarterly Journal of Mathematics*, **18** 1947, pp. 167-177.
- [11] S. Tomotika, Z. Hasimoto, and K. Urano, "The Forces Acting on an Aerofoil of Approximate Joukowski Type in a Stream Bounded by a Plane Wall", *Quart. Journ. Mech. and Applied Math.*, **4** 1951, pp. 289-307.
- [12] S. Tomotika, K. Tamada, and H. Umemoto, "The Lift and Moment Acting on a Circular-Arc Aerofoil in a Stream Bounded by a Plane Wall", *Quarterly Journal of Mechanics and Applied Mathematics*, **4** 1951, pp. 1-22.
- [13] J. Katz, "Calculation of the Aerodynamic Forces on Automotive Lifting Surfaces", *Journal of Fluids Engineering*, **107** Dec. 1985, pp. 438-443.
- [14] R. C. Chang, "An Experimental Investigation of Dynamic Ground Effect", *Ph.D. Dissertation, Department of Aerospace Engineering, University of Kansas, Lawrence, Kansas, April 1985*.
- [15] R. C. Chang and V. U. Muirhead, "Effect of Sink Rate on Ground Effect of Low-Aspect-Ratio Wings", *Journal of Aircraft*, **24** March 1987, pp. 176-180.
- [16] A. O. Nuhait, "Numerical Simulation of Feedback Control of Aerodynamic Configurations in Steady and Unsteady Ground Effects", *Ph.D. Dissertation, Department of Engineering Science and Mechanics, Virginia Polytechnic Institute and State University, Blacksburg, Virginia, Oct. 1988*.
- [17] A. O. Nuhait and D. T. Mook, "Numerical Simulation of Wings in Steady and Unsteady Ground Effects", *Journal of Aircraft*, **26** Dec. 1989, pp. 1081-1089.
- [18] D. T. Mook and A. O. Nuhait, "Simulation of the Interaction Between Aerodynamics and Vehicle Dynamics in General Unsteady Ground Effects", *AIAA Paper No. 89-1498, Intersociety Advanced Marine Vehicles Conference, June 5-8, 1989, Washington, D.C.*
- [19] G. T. Kemmerly, J. W. Paulson, Jr., and M. Compton, "Exploratory Evaluation of Moving-Model Technique for Measurement of Dynamic Ground Effects", *Journal of Aircraft*, **25** June 1988, pp. 557-562.
- [20] P. H. Lee, C. E. Lan, and V. U. Muirhead, "Experimental Investigation of Dynamic Ground Effect", *Journal of Aircraft*, **26** June 1989, pp. 497-498.
- [21] M. J. Kim, "Applications of Panel Methods for Subsonic Aerodynamics", *Ph.D. Thesis, Engineering Science and Mechanics Dept., Virginia Polytechnic Institute and State University, Blacksburg, VA., Jan. 1985*.

- [22] B. Dong, "Numerical Simulation of Two-Dimensional Lifting Flow", *M.S. Thesis, Engineering Science and Mechanics Dept., Virginia Polytechnic Institute and State University, Blacksburg, VA., Oct. 1987.*
- [23] D. T. Mook, S. Roy, G. Choksi, and B. Dong, "Numerical Simulation of the Unsteady Wake behind An Airfoil", *Journal of Aircraft*, **26** June 1989, pp. 509-514.
- [24] K. Karamcheti, *Principles of Ideal-Fluid Aerodynamics*. Malabar, Florida: R.E. Krieger Publishing Co., 1980.
- [25] J. Abbot and A. E. von Doenhoff, *Theory of Wing Sections*. New York, N.Y.: Dover, 1959.

Paper Received 22 May 1993; Revised 13 October 1993; Accepted 20 October 1993.